Accepted Manuscript

Effects of MgO on dielectric relaxation and phase transition study of the ceramic matrix $BaBi_4Ti_4O_{15}$

C.B. Gozzo, A.J. Terezo, E.H.N.S. Thaines, A.J.M. Sales, R.G. Freitas, A.S.B. Sombra, M.M. Costa

PII: S2468-2179(18)30231-4

DOI: https://doi.org/10.1016/j.jsamd.2018.12.008

Reference: JSAMD 199

To appear in: *Journal of Science: Advanced Materials and Devices*

Received Date: 9 November 2018

Revised Date: 21 December 2018

Accepted Date: 29 December 2018

Please cite this article as: C.B Gozzo, A.J. Terezo, E.H.N.S. Thaines, A.J.M. Sales, R.G. Freitas, A.S.B Sombra, M.M. Costa, Effects of MgO on dielectric relaxation and phase transition study of the ceramic matrix $BaBi_4Ti_4O_{15}$, *Journal of Science: Advanced Materials and Devices*, https://doi.org/10.1016/j.jsamd.2018.12.008.

Effects of MgO on dielectric relaxation and phase transition study of the ceramic matrix $BaBi_4Ti_4O_{15}$

C.B.Gozzo[1†], A.J. Terezo[1], E.H.N.S. Thaines[1], A.J.M. Sales[2], R.G. Freitas[1*], A.S.B.Sombra[3], M.M. Costa[3,4]

[1]Chemistry Department, Federal University of Mato Grosso, ICET-UFMT, 78060-900 Cuiabá, MT, Brazil

[2]I3N and Physics Department, Aveiro University, Campus Universitário de Santiago, Aveiro, Portugal.

[3]Physics Department, Federal University of Ceará, UFC, 60455-73, Brazil

[4]Institute of Physics, LACANM, UFMT, 78060-900 Cuiabá, MT, Brazil

†Present address: Departament of Chemistry, Federal University of São Carlos, São Carlos, SP,13565-905, Brazil

*Corresponding author: rgfreitas@ufmt.br

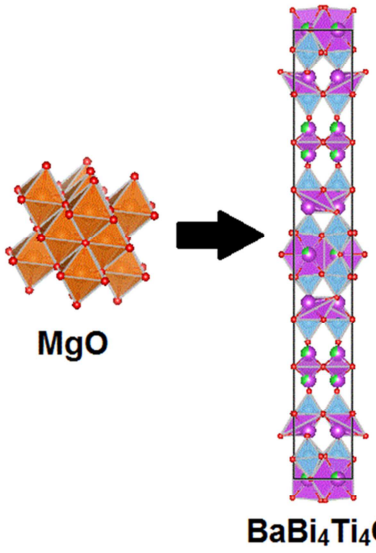
MgO
BaBi4Ti4O15

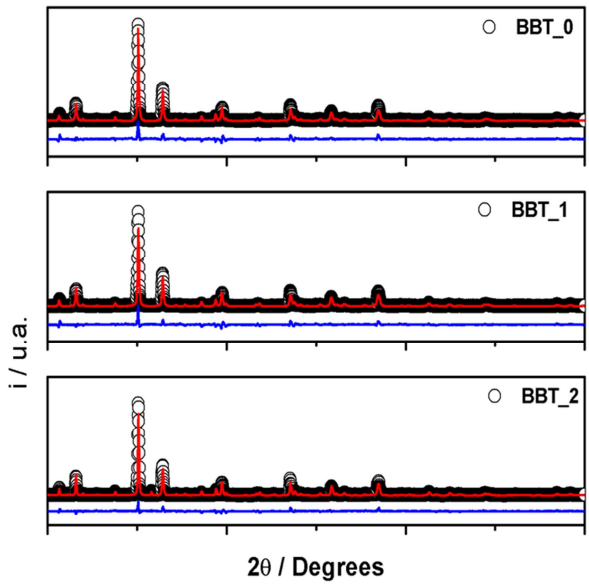
BBT_0
BBT_1
BBT_2
i / u.a.
2θ / Degrees

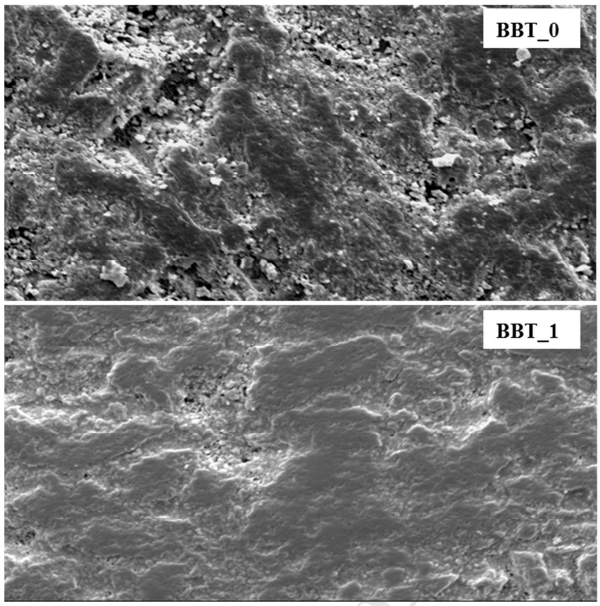
BBT_0
BBT_1

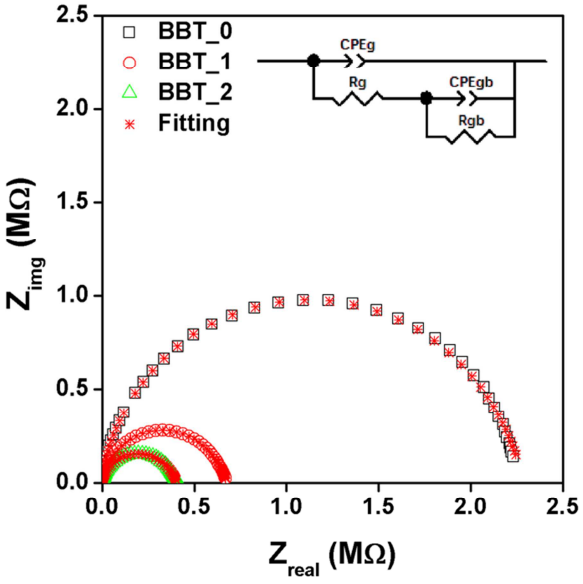
BBT_0
BBT_1
BBT_2
Fitting
CPEg
Rg
CPEgb
Rgb
Z_img (MΩ)
Z_real (MΩ)
0.0
0.5
1.0
1.5
2.0
2.5

Effects of MgO on dielectric relaxation and phase transition study of the ceramic matrix $BaBi_4Ti_4O_{15}$

Abstract

$BaBi_4Ti_4O_{15}$ ceramics doped with magnesium oxide in the weight concentration of 1 and 2 %, were prepared by the solid-state reaction method. X-ray diffraction analysis and impedance spectroscopy measurements were employed to study the influence of the structural characteristics on the electrical properties. The formation of the orthorhombic phase for all samples with a decrease in the unit cell volume was due to insertion of Mg^{2+} into Ti^{4+} sites. With the increase of magnesium oxide amount there was a decrease in the value of the complex impedance, both real (Z_{Real}), $4.75x10^7$ Ω to $6.68x10^6$ Ω, and imaginary ($-Z_{Img}$), $2.13x10^7$ Ω to $2.22x10^6$ Ω, respectively for samples BBT - 0 and BBT - 2. Using an equivalent circuit including the contribution of grain and grain-boundaries, it was observed activation energies of 1,169 and 0.874 eV for the grain and 1.320 and 0.981 eV for the grain boundary for samples BBT - 0 and BBT - 2, respectively. The replacement of Mg^{2+} into Ti^{4+} sites promotes a shift of the temperature of the dielectric constant maximum (*Tm*), measured at a fixed frequency, to higher temperatures.

Keywords: Doped $BaBi_4Ti_4O_{15}$ ceramics; dielectric relaxation; phase transition; impedance spectroscopy; ionic conductivity

1. Introduction

Relaxor ferroelectric materials are interesting technological materials due to properties such as the diffuse phase transition, high dielectric permittivity and strong electrostriction. These properties enhance the potential to use this material in a wide range of device applications like transducers or memory elements [1, 2, 3]. It is also known that the behavior of materials with ferroelectrics properties features a strong dependence on frequency in the region of the diffuse phase transition. However, the physical properties associated to these systems are still not completely understood [4, 5, 6].

The importance of studying the bismuth layer-structured ferroelectric ceramics (BLSFs) attracted considerable attention in the last years, with the formation of materials with different structures and with potential applications in non-volatile random access memory (NVRAM) and high temperature piezoelectric devices. The barium bismuth titanate ceramics (BBT) modified with Ce[7], Nb [8], Sm [6], La [9, 10]or with an excess of Bi_2O_3 [4,11]have shown a relaxor behavior, with strong dependence on the frequency. These materials present quite different dielectric constant values under the same measurement conditions, showing that the elements inserted into the structure of BBT present a strong influence on this physical property. Studies about the structural and electrical properties of pure BBT have shown a diffuse phase transition around 400 ^{o}C and the maximum value of dielectric constant moves to higher temperatures with increased frequency, showing a dependence on the dielectric constant with temperature, frequency and material preparation conditions [12, 13, 14].

The BBT structure follows a general formula of $(Bi_2O_2)^{2+}(A_{m-1}B_mO_{3m+1})^{2-}$, where A represents the ions with dodecahedral coordination, B the cations in the octahedral coordination and m is an integer representing the number of BO_6 octahedrons in the pseudo perovskite $(A_{m-1}B_mO_{3m+1})^{2-}$ layers existing between the $(Bi_2O_2)^{2+}$ layers. This material is polycrystalline and belongs to the Aurivillius family.

The dielectric properties, analyzed by impedance spectroscopy, is a convenient tool to characterize the different electrically active regions and their interfaces, allowing the separation of bulk, grain boundary, and electrode polarization contribution. Furthermore, it can be used to

investigate the dynamics of bond or mobile charges in the bulk or interfacial regions of any kind of solid or liquid material: ionic, semiconducting, mixed electronic-ionic and insulators. To extract so meaningful information, it is essential to model the experimental data with a proper equivalent electrical circuit. One example is the possible extraction of the relaxation frequency (ω_{max}) of the material, which, at a given temperature, is an intrinsic property of the material, independent of its geometry. The analysis of the dielectric properties was made using different formalisms, impedances, modulus, permittivity, etc, and the achievement of the activation energy related with the relaxation phenomena.

Moreover, and specifically to ceramic materials containing grains and grain boundary regions, which individually have very different physical properties, can be filtered using those formalisms. For example, in polycrystalline materials, impedance formalism emphasizes the grain boundary conduction process, while bulk effects on the frequency domain dominate in the dielectric modulus formalism.

In this study we report the influence of MgO content in the structure and the dielectric properties of BBT using these tools. This work shows that MgO concentration modifies the value of a dielectric constant with frequency and phase transition temperature. Simultaneous analysis of the complex impedance, electric modulus and appropriate equivalent circuit models, two values of relaxations were identified in the frequency range used at high temperatures. The value of resistivity associated with grain and grain boundary was determined and the activation energy obtained for both cases.

2. Experimental procedure

$BaBi_4Ti_4O_{15}$ ceramics doped with magnesium oxide in concentrations of 0, 1 and 2 wt% (named as: BBT_O, BBT_1 and BBT_2), were prepared using the solid-state reaction method. The raw materials (high purity grade BaO (99.9%), Bi_2O_3(99.9%), TiO_2(99.9%) and MgO (99.9%)), after weighted in the appropriate amounts, were homogenized in a planetary ball mill system (Pulverisette 5-Fritsch) using reactors and spheres of zirconium oxide. The grinding was performed at a speed of 360 rpm for 6hours and after calcined at 850 °C for 3hours in alumina crucible in order to promote for the BBT formation. The samples were mixed with a small amount of PVA (polyvinyl alcohol),then pressed into pellets of about 1 mm in thickness and 12

mm in diameter using a uniaxial pressure system (a pressure of 346.8 MPa for 5 min was applied). The pellets were sintered at 950 ºC, in air, for 3hours (heating rate 5^{o}C/min) and then cooled to room temperature (cooling rate 5 ^{o}C/min).

The crystal phase identification and characterization were done using a Bruker-D8 Advance powder X-Ray Diffractometer (XRD), operating with CuK_{α} radiation (λ = 0.154 nm) and using the 2θ range from 20 up to 80°, with increment and time for step of 0.02 and 0.2, respectively. The Rietveld refinement was performed using software DBWS9807a, through the interface DBWStools 2.4 [15].

For the electrical characterizations and temperature dependent dielectric properties a Solartron 1260 coupled to a temperature programmable furnace was used. For this measurement the pellets were coated with silver paste on both sides of the circular surface and cured for 1hour at 200 °C. The measurements were done in the frequency range of 1 Hz to 1 MHz and temperature from 30 up to 530 °C. The complex impedance data [16] was analyzed in terms of complex dielectric permittivity (ε^*), complex impedance (Z^*) and dielectric modulus (M^*), which are related to each other as: $Z^*=Z_{Real}-jZ_{Img}$; $M^*=1/\varepsilon^*(\omega) = j(\omega C_0)Z^*=M_{Real} + jM_{Img}$, where ($Z_{Real}$, M_{Real}) and (Z_{Img}, M_{Img}) are the real and imaginary components of impedance and modulus, respectively, $j = \sqrt{-1}$ the imaginary factor and ω is the angular frequency, $\omega = 2\pi f$, $C_0=\varepsilon_0 A/d$ is the geometrical capacitance, ε_0 is the permittivity of vacuum, A and d are the area and thickness of the pellets. The impedance spectra were analyzed using ZView 3.1, fitting by means of a complex, non-linear least squares algorithm associated to equivalent electrical circuits.

Were realized the microstructural characterization and energy dispersive X-Ray (EDX) analysis in the samples fractured and polished sample using a Shimadzu SSX-550 scanning electron microscopic (SEM).

3. Results and Discussion

3.1 Structural properties

X-ray diffraction is a powerful technique to study structural properties of materials. In this sense, Fig 1(a-c) shows the Rietveld refinement patterns obtained for BBT_O, BBT_1 andBBT_2. The diffracted peaks of all samples are well indexed with the orthorhombic structure with space group $A2_1am$ (ICSD - 150928).

Aurivillius phase has highest diffraction and peaks at (112m+1) [10, 12]. The intense peaks about 30° (119), are an indication of the number of perovskites layers (m = 4). The difference between the BBT-0 and the calculated data was close to zero ($Y_{observed}$ - $Y_{calculated}$) and its statistical parameters (χ^2 = 2.24) are in good agreement with the structure found in previous works [17,18]. Therefore, the refinement concludes that the structure of the BBT_O sample is orthorhombic ($A2_1am$), and the lattice parameters are$a$ = 5.45712(0) Å, b = 5.45172(8) Å and c = 41.88594(0) Å, as presented in Table 1.

Previous studies show that the substitution of the Mg^{2+} in the perovskites of the $BaTiO_3$ occurs at Ti^{4+} site and not in the Ba^{2+} site, since the difference between the ionic radius of Ba^{2+}it is much higher that of Mg^{2+} [19, 20]. According to the data of Rietvield refinement presented in Table 1, it is observed that the volume of unit cell decrease in function of the MgO amount. An increase in volume of the unit cell should be expected which is assigned to the fact that the ionic radius of Mg^{2+} (0.72 Å) is higher than Ti^{4+} (0.605 Å) [19]. However, Wang, et al. [21] also describes this behavior as due to the increase in the number of oxygen vacancies generated by the incorporation of Mg^{2+} ions.

3.2 Scanning electron microscopy

SEM images of the fractured and polished samples are shown in Fig. 2 (a-c) for samples BBT_O, BBT_1 and BBT_2.This analysis was performed to observe the contribution of MgO in sintering properties of BBT. It is observed an increase in the density of the samples with MgO concentration. The addition of Mg promotes an increase in the sinterability of the samples, how observed by Kai et al.[35]. For a pure sample (BBT_O), the resistance of the grain (bulk) is lower than the grain boundary, and the addition of Mg to the structure leads to a decrease of the grain (bulk) resistance when compared with the one of the grain boundary, as observed in table 2, these results are observed in the electrical properties. This effect can be attributed that addition

of Mg promotes an increase in grain size, consequently decrease its resistance with increase of Mg content. Fig. 2d shows the EDX spectra, where the composition of samples BBT_O, BBT_1 and BBT_2 is qualitatively observed. With the increase of MgO, it is possible to observe the presence of Mg, besides the elements Bi, Ba, Ti and O.

3.3 Electrical Properties

3.3.1 Impedance analysis

Fig. 3 (a-c) shows the temperature dependence of the real part of impedance (Z_{Real}) with frequency at different temperature for BBT_O, BBT_1 and BBT_2.

The results clearly show that the addition of MgO oxide decreases the value of the impedance with increasing temperature and frequency, which indicates the possibility of an increase in the ac conductivity of the materials. However, there is a decrease of impedance (approximately one order of magnitude) in all curves but it merges in the higher-frequency region (>10^3Hz) independently on the temperature. The merger of real part of impedance in the higher-frequency domain suggests a possible release of space charge and a consequent lowering of the barrier properties in the materials [22].

Fig. 4(a-f) shows the temperature dependence of the imaginary part of impedance (Z_{Img}) with frequency at different temperature for BBT_O, BBT_1 and BBT_2.The value of Z_{Img} varies with frequency and at a in a maximum value at a particular frequency known as dielectric relaxation frequency (ω_{max}), being more noticeable for temperatures above 350 ^oC. The normalization of the imaginary impedance component facilitates to observe the dielectric relaxation frequency (Fig. 4(d-f)).

The peaks position shifts towards higher frequencies with the increase of temperature and the asymmetric broadening of the peaks suggests a pre-relaxation time with two equilibrium positions [23]. The absence of peaks in the low-temperature range (up to 340 ^oC) for all the samples (BBT_O, BBT_1 and BBT_2) in the loss spectrum suggests the lack of current dissipation in this temperature region. The pattern shows the presence of peaks at a particular frequency that describes the type and strength of electrical relaxation phenomenon and it is a clear proof of temperature dependent relaxation. Further, the magnitude of Z_{Img} decreases with the increase of the temperature and increase of MgO amount the peak frequency shifts towards

higher frequencies, and normally converges to a same value in the high-frequency region (>10^3 Hz), which indicates an accumulation of space charge [24].

In the samples analyzed in this work it was observed that increasing the MgO content, Z_{Img} presents a maximum, whose frequency shifts to higher frequencies and in the higher frequency region converges to a same value, which indicates the presence of space charge polarization [25]. The value of Z_{Imgmax} shifts to higher frequency side on increasing MgO concentration in the materials. A significant increase in the broadening of the peaks with increase in doping concentration suggests the enhancement of electrical relaxation phenomenon in the materials.

3.3.2 Equivalent circuit analysis

Fig. 5(a-c) and its inset compares the variation of complex impedance spectrum Z_{Real} versus Z_{Img} (called as Nyquist plot) with the fitted data for BBT_O, BBT_1 and BBT_2 compounds obtained at different temperatures (>350 ^oC) over a wide range de frequency (10 Hz – 1 MHz).

The plots indicate the presence of two semicircles, whose amplitude decreases with the increase of the temperature. The semicircle at low frequencies is related with grain-boundary relaxation and the high frequency semicircle with bulk relaxation [26].The experimental data was fitted using commercially available software ZView 3.1 for non-Debye response and the results are show in Fig. 5(a-c) and Table 2.

The overlapping of the two semicircular arcs of the impedance spectrum was adjusted to an equivalent circuit shown in the Fig. 6.

It was assumed an ideal case where both grain and grain boundary characteristics follow a non-Debye behavior. The equivalent circuit proposed to analyze the experimental results, is constituted by the following elements: bulk resistance (R_g), constant phase element related with the grain (bulk) (CPE_g), grain boundary resistance (R_{gb}), and constant phase element of the grain boundary (CPE_{gb}). Using this circuit we managed to obtain a good fit of the experimental data. With the parameters used in the circuits and using the adjustment program, was possible to extract all the information from the material, as the resistances, the capacitance, alpha (α_g and

α_{gb})and relaxation times (τ_g and τ_{gb}) these results are shown in the Table 2 for five different temperatures.

Analyzing the relaxation times values, one can notice that they decrease with the increase of temperature and increase of MgO content (Table2).

3.3.3 Dielectric constant analysis

The analysis of the dielectric constant behavior as a function of the temperature is a useful tool to identify phase transitions. Fig. 7(a-c) show the temperature dependence of the dielectric constant (ε_{Real}) for several frequencies, revealing the presence of a peak during the heating stage.

It is also visible that the maximum value of the dielectric constant, for each frequency, decrease in (ε_{Real}) with increasing frequency, and a small shift in *Tm* (temperature at which one has the maximum dielectric constant) is noted with increasing frequency. It is also noted that the maximum value of constant dielectric increases with increasing concentration of MgO and the peak shifts to higher temperature (Fig. 7d),which signifies the relaxor behavior of the present ceramics. This result shows that the dielectric constant exhibits a broad diffused transition around the phase transition temperature, with a strong dependence on frequency and MgO concentration. It is suggested that this can be assigned to the structural transformation that promotes the formation of a ferroelectric phase, i.e., in the present case the structural transformation from orthorhombic to tetragonal [17]. The MgO concentration leads to strong variation of the maximum value of dielectric constant when compared to a pure sample of BBT, which shows a dielectric constant value of about ~190 and the *Tm* value of 435 ^{o}C, which are in agreement with the literature [8,13, 7, 27].

3.3.4 Conductivity analysis

Fig. 8(a-c) show the conductivity profile ($\sigma(\omega) = \omega\varepsilon_0\varepsilon_{Img}$)as a function of frequency at several temperatures for BBT_O, BBT_1 and BBT_2 samples. Visible is a dispersion of the

conductivity for all frequencies and all samples and an increasing with temperature and MgO concentration.

In the low frequency region, the conductivity shows a frequency-independent behavior (*dc* conductivity) and in the higher frequencies region it shows a dependence like $A.\omega^{n(T)}$ (*ac* conductivity), where A is a constant, ω is angular frequency and n(T) is a temperature dependent exponent ($0<n \leq 1$) [28] representing the degree of interaction between mobile ions with lattice. This behavior indicates that the conductivity presents a relaxation behavior associated to mobile charge carriers. Considering the low-frequency region, it is possible by extrapolation to calculate dc conductivity value. This value increase with the increase of temperature and can be used to estimate the value of the energy of the charge carriers.

3.3.5 Modulus analysis

The modulus formalism was used to better understand the relaxation mechanisms present in BBT with different contents of MgO. It is known that in polycrystalline materials, impedance formalism emphasizes the grain boundary conduction process, while bulk effects on the frequency domain dominate in the electric modulus formalism [29, 30]. The use of modulus spectroscopy plot is particularly useful for: i) separating the components with similar resistance but different capacitance, ii). to detect electrode polarization, iii) grain boundary conduction effect, iv) bulk properties, v) electrical conductivity and vi) relaxation time. The main advantage of the dielectric modulus formalism is that the electrode effects are suppressed because usually they are related with high capacities active at low frequencies, which are minimized with this formalism.

The variation of the real part of electric modulus (M_{Real}) is very low in the low frequency region (approaching zero). As frequency increases the M_{Real} value increases and reaches a maximum at higher frequencies for all temperatures associated to a lack of restoring force governing the mobility of charge carriers under the action of an induced electric field [31,32].

Fig. 9(a-c) and its inset shows the variation of imaginary part of dielectric modulus (M_{Img}) versus frequency at different temperatures for BBT_O, BBT_1 and BBT_2 samples, respectively.

In all samples the curves present similar behavior, where is clearly visible the *Tm* temperature. At temperatures below the *Tm*, the maximum value of the peak decrease and the peak position moves to higher frequencies with increase in temperature, indicating that the associated capacitance is increasing. At temperatures above *Tm*, the peak height starts to increase indicating a decrease in the related capacitance. Results in the literature show that the BBT is a ferroelectric compound with a phase transition around 417 ^{o}C (at 100 kHz) [33,34]. The results shown here are in full agreement with those data for BBT_O sample. Before and after *Tm*, the relaxation frequency obeys the Arrhenius law, however, there is an anomaly around this temperature, as shown in Fig. 10.

3.3.6 Activation energy analysis

From the results presented in Fig. 8, for the dc conductivity, associated with the 1Hz response, all temperatures follow the Arrhenius relation ($\sigma = \sigma_0 \exp\left[-\frac{E_a}{kT}\right]$) in the two regions before and after *Tm*, where $\sigma_0$is a pre-exponential factor, E_a is the activation energy; k is the Boltzmann constant; and T the absolute temperature. Fig. 10 shows the results for BBT_1 of the value of the activation energy, calculated from the conductivity (dc) in frequency 1Hz at different temperatures. For other samples, the results are showed in Table 3.

From the results presented in Fig. 9 we found the frequency of the peak corresponding to each temperature in all samples and fitted those results with an Arrhenius relation ($f = f_0 \exp\left[-\frac{E_a}{kT}\right]$, where f_0 is a pre-exponential factor, E_a is the activation energy, k is the Boltzmann constant and T the absolute temperature)in the regions before and after of the value *Tm*. For the sample BBT_1 the value of activation energy is shown in Fig. 10. For the other samples the results are shown in Table 3.

From the results presented in Table 2 for all samples at different temperatures, we separated the values of R_g and R_{gb}, obtained from fittings and therefore we could estimate the resistivity values before and after *Tm*, for grain and grain-boundary at different temperatures. Fig. 11 shows the Arrhenius plot of the resistivity for BBT_1 sample, from where the activation energies for the electrical conduction processes could be extracted. For the sample

BBT_1,around 425 ^{o}C, there is a change in the activation energies (Fig. 11). The difference between those values is associated with the ferroelectric phase transition which takes place in that temperature range.

The values of activation energy related with the grain contribution (Table 3) are comparable with the ones obtained from the relaxation peak frequency analysis (Fig. 10) and should be assigned to the oxygen vacancies in bismuth-layered oxides that occurs from the oxygen loss during the sintering process in order to balance the charge mismatch due to the existence of bismuth vacancies.

These results show that activation energies related to relaxation process (Fig. 10 and Table 3) are slightly higher than those obtained from conduction processes (Fig. 10 and Table 3) in the temperature range and with different concentration of MgO. Generally, the relaxation process does not govern the electrical conduction. At high temperatures, different types of charge carriers could contribute to the electrical conduction, although these may not be related to the dielectric relaxation or to the dielectric polarization. For example, the electrons released from the oxygen vacancy ionization are easily thermal activated and become conducting electrons, however the dipoles form by the oxygen vacancies and electrons on the grain boundaries can easily trap those conduction electrons and block the ionic conduction across the grain-boundaries promoting an increase of the resistivity.

The Table 3 shown that value of activation energy obtained from all samples below *Tm* and above *Tm*. The difference between values are in agreement with another results found in the literature [12, 13].

4. Conclusion

The polycrystalline ceramic BBT was prepared by a conventional solid state reaction technique at the sintering temperature of 950 ^{o}C. Phase compound is confirmed by X-ray diffraction analysis which shows that the BBT with structure orthorhombic and confirm by be well fitted to a orthorhombic BBT structure.

Also, the impedance studies exhibit the presence of grain (bulk) and grain boundary effects, and existence of a NTCR in the material. With the increase of magnesium oxide amount there was a decrease in the value of the complex impedance, both real (Z_{Real}), $4.75x10^7$ Ω to $6.68x10^6$ Ω, and imaginary ($-Z_{Img}$), $2.13x10^7$ Ω to $2.22x10^6$ Ω, respectively for samples BBT - 0 and BBT - 2. The equivalent circuit was proposed to analyze the experimental results. It was possible to extract all the information from the material as the resistances and capacitance of the material before and after of phase transition. It was possible separate the effects of grain (bulk) and grain boundary. It was possible obtain the activation energies of 1,169 and 0.874 eV for the grain and 1.320 and 0.981 eV for the grain boundary for samples BBT - 0 and BBT - 2, respectively. The modulus formalism shown a transition temperature *Tm* dependent on the MgO content and frequency. This was confirmed by the dielectric constant versus temperature results. The high phase transition temperature shifts to higher temperatures with increasing of MgO concentration. Moreover, complex impedance and modulus electric showed that a dielectric relaxation in the material of the non-Debye type and phase transition dependent of content of MgO in the matrix ceramic of BBT is present.

The difference between activation energy of the samples, estimated from the frequency peak (modulus) and resistivity for grain (fitted) can be explained because the modulus, consider only effects associated with conduction processes that are thermally activated. The activation energy obtained from contribution grain is less than obtained from contribution grain boundary in all samples. This values indicating that material can be used in electronics device.

Acknowledgements

This work was partly sponsored by CNPq (427161/2016-9), CAPES and FAPEMAT (214599/2015)Brazilian funding agencies.

Compliance with Ethical Standards:

This study was funded by CNPq, CAPES and FAPEMAT.

Conflict of Interest: The authors declare that they have no conflict of interest.

5. Reference

[1] R. Blinc, Order and Disorder in Perovskites and Relaxor Ferroelectrics, Struct. Bond. 124 (2007) 51-67. https://doi.org/10.1007/430_2006_050

[2] S.E. Park, T.R. Shrout, Ultrahigh strain and piezoelectric behavior in relaxor based ferroelectric single crystals, J. Appl. Phys. 82 (1997) 1804-1811. https://doi.org/10.1063/1.365983

[3] S.K. Rout, E. Sinha, A. Hussian, J.S. Lee, C.W. Ahn, I.W. Kim, S.I. Woo, Phase transition in ABi$_4$Ti$_4$O$_{15}$ (A=Ca, Sr, Ba) Aurivillius oxides prepared through a soft chemical route, J. Appl. Phys. 105 (2009) 024105-024106. https://doi.org/10.1063/1.3068344

[4] A. Khokhar, P. K. Goyal, O.P. Thakur, K. Srenivas, Effect of excess of bismuth doping on dielectric and ferroelectric properties of $BaBi_4Ti_4O_{15}$ ceramics, Ceram. Internat. 41 (2015) 4189-4198. https://doi.org/10.1016/j.ceramint.2014.12.103

[5] C.L. Diao, H.W. Zheng, Y.Z. Gu, W.F. Zhang, L. Fang, Structural and electrical properties of four-layers Aurivillius phase $BaBi_{3.5}Nd_{0.5}Ti_4O_{15}$ ceramics, Ceram. Internat. 40(4) (2014) 5765-5769. https://doi.org/10.1016/j.ceramint.2013.11.015

[6] P. Fang, P. Liu, Z. Xi, Quantitative description of the phase transition of Aurivillius oxides Sm modified BaBi4Ti4O15 ceramics, Phys. B: Cond. Matter. 468(9) (2015) 34-38. https://doi.org/10.1016/j.physb.2015.03.033

[7] C.L. Diao; J.B. Xu; H.W. Zheng; L. Fang; Y.Z. Gu; W.F. Zhang, Dielectric and piezoelectric properties of cerium modified $BaBi_4Ti_4O_{15}$ ceramics, Ceram. Internat. 39(6) (2013) 6991-6995. https://doi.org/10.1016/j.ceramint.2013.02.036

[8] J.D. Bobic, M.M. Vijatovic, J. Banys, B.D. Stojanovic, Electrical properties of niobium doped barium bismuth-titanate ceramics, Mater. Res. Bull. 47 (2012) 1874-1880. https://doi.org/10.1016/j.materresbull.2012.04.069

[9] A. Khokhar, P. K. Goyal, O.P. Thakur, A.K. Shukla, K. Sreenivas, Influence of Lanthanum Distribution on Dielectric and Ferroelectric Properties of $BaBi_{4-x}La_xTi_4O_{15}$ Ceramics, Mater. Chem. Phys. 152(2015) 13-25. https://doi.org/10.1016/j.matchemphys.2014.11.074

[10] A. Chakrabarti, L. Bera, Effect of La-substitution on the structure and dielectric properties of BaBi4Ti4O15 ceramics, J. Alloys Compd. 505 (2010) 668-674. https://doi.org/10.1016/j.jallcom.2010.06.105

[11].P.M.V.Almeida,C.B.Gozzo, E.H.N.S.Thaines, A.J.M.Sales, R.G.Freitas, A.J.Terezo, A.S.B.Sombra, M.M.Costa, Dielectric relaxation study of the ceramic matrix $BaBi_4Ti_4O_{15}$:Bi_2O_3, Mater. Chem. Phys. 205 (2018) 72-83. https://doi.org/10.1016/j.matchemphys.2017.10.069

[12] J.D. Bobić, M.M. Vijatović, S. Greičius, J. Banys, B.D. Stojanović, Dielectric and relaxor behavior of BaBi4Ti4O15 ceramics, J. Alloys Compd. 499(2010) 221-226. https://doi.org/10.1016/j.jallcom.2010.03.171

[13] S. Kumar, K. B. R. Varma, Dielectric relaxation in bismuth layer-structured BaBi4Ti4O15 ferroelectric ceramics, Current Applied Physics. 11 (2011) 203-210. https://doi.org/10.1016/j.cap.2010.07.008

[14] P. Fang, H. Fan, Z. Xi, W. Chen, Studies of structural and electrical properties on four-layers Aurivillius phase BaBi4Ti4O15, Solid. State Comm. 152 (2012) 979-983. https://doi.org/10.1016/j.ssc.2012.03.007

[15] L.Bleicher, J.M. Sasaki, C.O.P.Santos, Development of a graphical interface for the Rietveld refinement program *DBWS*, J. appl. Cryst. 33 (2000) 1189-1189. https://doi.org/10.1107/S0021889800005410

[16] J.R. MacDonald, Impedance Spectroscopy, Wiley, New York, 1987.

[17] B.J. Kennedy, Q. Zhou, Ismunandar, Y. Kubota, K. Kato, Cation disorder and phase transition in the four-layer ferroelectric Aurivillius phase $ABi_4Ti_4O_{15}$ (A=Ca, Sr, Ba, Pb), J. Sol. Stat. Chem. 181 (2008) 1377 – 1386. https://doi.org/10.1016/j.jssc.2008.02.015

[18]B.J. Kennedy, Y. Kubota, B.A. Hunter, Ismunandar, K. Kato, Structural phase transitions in the layered bismuth oxide BaBi4Ti4O15, Solid State Commun. 126 (2003) 653 – 658. https://doi.org/10.1016/S0038-1098(03)00332-6

[19] A. Tkach, P.M. Vilarinho, A. Kholkin, Effect of Mg doping on the structural and dielectric properties of strontium titanate ceramics, Appl. Phys. A 79 (2004) 2013 – 2020. https://doi.org/10.1007/s00339-003-2341-z

[20] J.S. Park, M.H. Yang, Y.H. Han, Effects of MgO coating on the sintering behavior and dielectric properties of $BaTiO_3$, Mater. Chem. and Phys. 104 (2007) 261 – 266. https://doi.org/10.1016/j.matchemphys.2007.02.092

[21]M. Wang, H. Yang, Q. Zhang, Z. Lin, Z. Zhang, D. Yu, L. Hu, Microstructure and dielectric properties of $BaTiO_3$ ceramic doped with yttrium, magnesium, gallium and silicon for AC capacitor application, Mater. Res. Bull. 60 (2014) 485 – 491. https://doi.org/10.1016/j.materresbull.2014.09.023

[22] A. Kumar, B.P. Singh, R.N. Choudhary, P. Awalendra, K. Thakur, Characterization of electrical properties of Pb-modified $BaSnO_3$ using impedance spectroscopy, Mater. Chem. Phys. 99 (2006) 150–159. https://doi.org/10.1016/j.matchemphys.2005.09.086

[23]S. Chatterjee, P.K. Mahapatra, R.N.P. Choudhary, A.K. Thakur, Complex impedance studies of sodium pyrotungstate – $Na_2W_2O_7$, Phys. Stat. Sol. 201(2004) 588-595. https://doi.org/10.1002/pssa.200306741

[24] S. Pattanayak, B.N. Parida, P.R. Das, R.N.P. Choudhary, Impedance spectroscopy of Gd-doped $BiFeO_3$ multiferroics, Appl. Phys. A. 112(2013) 387–395. https://doi.org/10.1007/s00339-012-7412-6

[25] J. Fleig, J. Maier, The polarization of mixed conducting SOFC cathodes: Effects of surface reaction coefficient, ionic conductivity and geometry, J. Eur. Ceram. Soc, 24 (2004) 1343-1347. https://doi.org/10.1016/S0955-2219(03)00561-2

[26] D.C. Sinclair, A.R. West, Impedance and modulus spectroscopy of semiconducting $BaTiO_3$ showing positive temperature coefficient of resistance, J. Appl. Phys. 66 (1989) 3850-3856. https://doi.org/10.1063/1.344049

[27] A. Khokhar, M.L.V. Mahesh, A. R. James, P.K. Goyal, K. Sreenivas, Sintering characteristics and electrical properties of BaBi4Ti4O15 ferroelectric ceramics, J. Alloys and Comp. 581 (2013) 150–159. https://doi.org/10.1016/j.jallcom.2013.07.040

[28] A.K. Jonscher, The 'universal' dielectric response, Nature. 267 (1977) 673-679. https://doi.org/10.1038/267673a0

[29] J. Liu, Ch-G. Duan, W-G. Yin, W.N. Mei, R.W. Smith, J.R. Hardy, Dielectric permittivity and electric modulus in $Bi_2Ti_4O_{11}$, J. Chem. Phys. 119 (2003) 2812. https://doi.org/10.1063/1.1587685

[30] P. Kumar, B. P. Singh, T. P. Sinha, N. K. Singh, A Study Of Structural, Dielectric And Electrical properties of $Ba(Nd_{0.5}Nb_{0.5})O_3$ Ceramics, Adv. Mat. Lett., 3(2) (2012) 143-148. https://doi.org/10.5185/amlett.2011.8298

[31] I.M. Hodge, M.D. Ingran, A.R. West, A new method for analysing the a.c. behaviour of polycrystalline solid electrolytes, J. Electroanal. Chem. 58 (1975) 429-432. https://doi.org/10.1016/S0022-0728(75)80102-1

[32] K.P. Padmastree, D.K. Kanchan, A. R. Kulkami, Impedance and Modulus studies of the solid electrolyte system $20CdI_2–80[xAg_2O–y(0.7V_2O_5–0.3B_2O_3)]$, where $1 \leq x/y \leq 3$, Solid State Ion. 177 (5-6) (2006) 475-482. https://doi.org/10.1016/j.ssi.2005.12.019

[33] R.Z. Hou, X.M. Chen, Y.W. Zeng, Diffuse ferroelectric phase transition and relaxor behaviors in Ba-based bismuth layer-structured compounds and La-substituted $SrBi_4Ti_4O_{15}$, J. Am. Ceram. Soc. 89 (2006) 2839e2844. https://doi.org/10.1111/j.1551-2916.2006.01175.x

[34] S. Kumar, K.B.R. Varma, Influence of lanthanum doping on the dielectric, ferroelectric and relaxor behaviour of barium bismuth titanate ceramics, J. Phys. D: Appl. Phys. 42 (2009) 075405. https://doi.org/10.1088/0022-3727/42/7/075405

[35] K.C. Kai, C.A.V.A. Machado, L.A. Genova, Influence of Zn and Mg Doping on the Sintering Behavior and Phase Transformation of Tricalcium Phosphate Based Ceramics, J. Marchi. Mater. Sci. Forum. 805 (2015) 706-711. https://doi.org/10.4028/www.scientific.net/MSF.805.706

Table 1 -Crystallographic parameters obtained using Rietveld refinement for BBT_O. BBT_1.andBBT_2 samples.$\alpha = \beta = \gamma = 90^o$.

LatticeParameters/(Å)	***a***	***b***	***c***	**Volume ($Å^3$)**
ICSD - 150928	5.4707(2)	5.4565(2)	41.865(11)	1249.71
BBT_O	5.45712(0)	5.45172(8)	41.8859(40)	1246.13
BBT_1	5.45906(5)	5.45226(9)	41.8231(20)	1244.83
BBT_2	5.46186(1)	5.44937(9)	41.7598(40)	1242.91

Table 2 - Extract parameters obtained using fitting procedure and circuit elements for BBT_O. BBT_1.andBBT_2 samples.

				BBT_O				
T (^{o}C)	**R_g (Ω)**	**CPE_g (F)**	**α_g**	**R_{gb}(Ω)**	**CPE_{gb}(F)**	**α_{gb}**	**τ_g(s)**	**τ_{gb}(s)**
370	5.9436E6	2.684E-10	0.9729	2.149E7	1.811E-9	0.5490	0.0016	0.0389
410	1.6107E6	3.058E-10	0.98037	5.386E6	1.529E-9	0.6514	4.925E-4	0.0082
450	5.372E5	2.767E-10	0.9876	1.754E6	1.374E-9	0.7092	1.486E-4	0.0024
490	2.557E5	2.141E-10	0.9906	6.353E5	1.653E-9	0.7206	5.475E-5	0.0010
530	1.746E5	1.494E-10	0.9931	2.776E5	2.639E-9	0.6920	2.609E-5	0.0007
				BBT_1				
T (^{o}C)	**R_g(Ω)**	**CPE_g(F)**	**α_g**	**R_{gb}(Ω)**	**CPE_{gb}(F)**	**α_{gb}**	**τ_g(s)**	**τ_{gb}(s)**
370	1.817E6	3.226E-10	0.9705	5.806E6	2.877E-9	0.6004	5.863E-4	0.01671
410	5.089E5	4.331E-10	0.9754	1.511E6	4.178E-9	0.6244	2.204E-4	0.00631
450	1.743E5	3.738E-10	0.9871	5.061 E5	4.835E-9	0.6382	6.517E-5	0.00245
490	7.390E4	2.58E-10	0.9935	1.993E5	8.612E-9	0.5940	1.906E-5	0.00172
530	4.362E4	1.817E-10	0.9935	9.578E4	1.754E-8	0.5481	7.925E-6	0.00168
				BBT_2				
T (^{o}C)	**R_g(Ω)**	**CPE_g(F)**	**α_g**	**R_{gb}(Ω)**	**CPE_{gb}(F)**	**α_{gb}**	**τ_g(s)**	**τ_{gb}(s)**
370	7.891E5	2.172E-10	0.97648	3.167E6	4.421E-9	0.5943	1.714E-4	0.014
410	3.587E5	3.512E-10	0.97472	9.874E5	7.239E-9	0.6046	1.259E-4	0.00715
450	1.102E5	5.221E-10	0.97939	2.982E5	1.073E-8	0.6301	5.753E-5	0.0032
490	3.840E4	5.433E-10	0.98509	1.097E5	1.607E-8	0.6310	2.086E-5	0.00176
530	2.240E4	3.462E-10	0.98847	5.440E4	2.389E-8	0.6056	7.756E-6	0.0013

Table 3 - Values of activation energy in all samples obtained of thef_{peak}(frequency peak).σ_{dc} (dc conductivity).ρ_g(resistivity of the grain) and ρ_{gb}(resistivity of the grain boundary)

Sample		BBT_O		BBT_1		BBT_2
	E_a<Tm eV	E_a>Tm eV	E_a<Tm eV	E_a>Tm eV	E_a<Tm eV	E_a>Tm eV
f_{peak}(Fig.8)	1.109	1.443	0.916	1.416	0.814	1.415
σ_{dc}(Fig.7)	1.174	1.099	1.206	1.008	1.197	0.864
ρ_g	1.169	0.788	1.123	0.941	0.874	0.874
ρ_{gb}	1.320	1.173	1.252	1.078	1.261	0.981

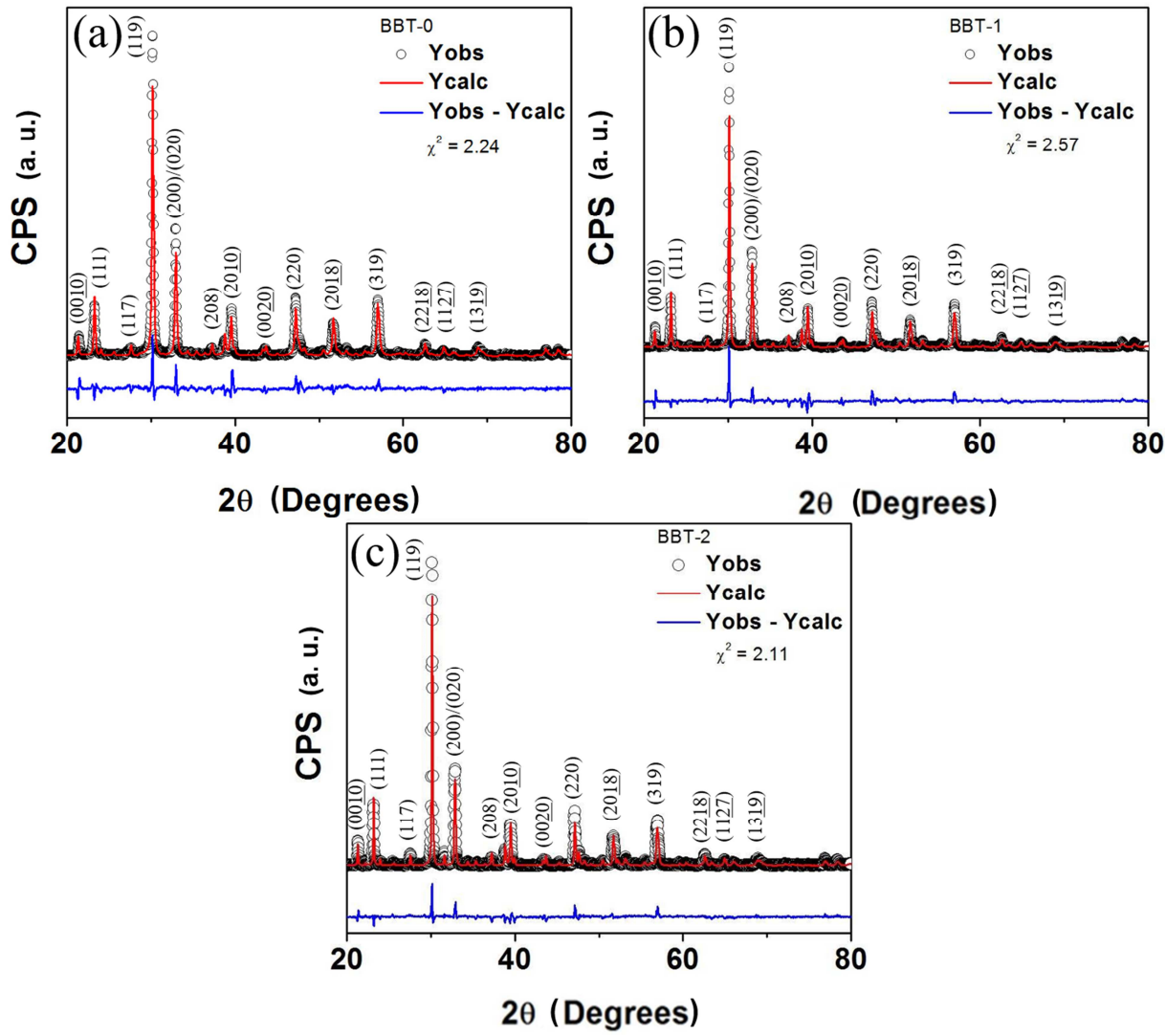

Figure 1 - Rietveld refinement pattern for (a) BBT_O; (b) BBT_1; and (c) BBT_2.

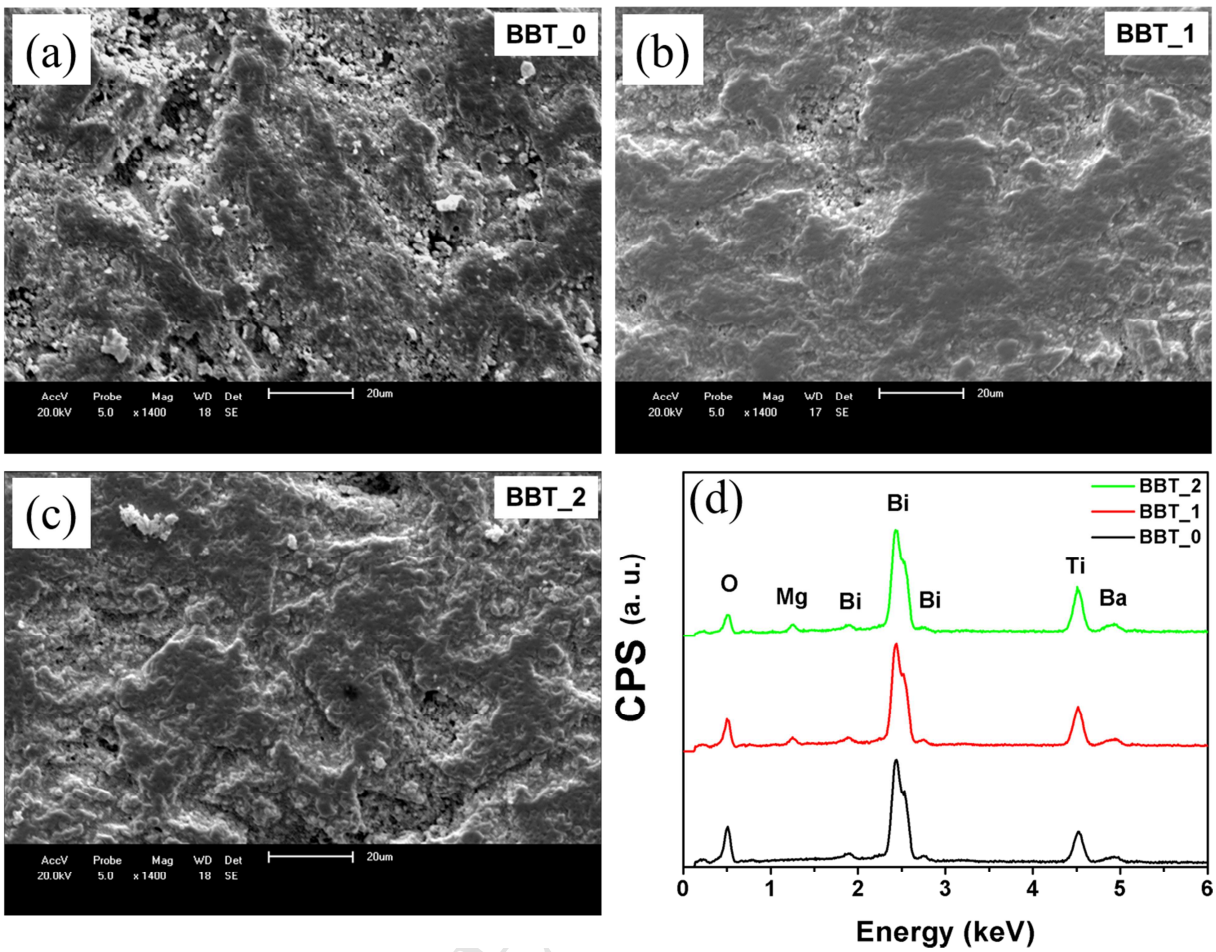

Figure 2 - Scanning electronic microscopy for (a) BBT_0, (b) BBT_1 and (c) BBT_2 samples. (d) EDX spectra with composition of samples BBT_O, BBT_1 and BBT_2.

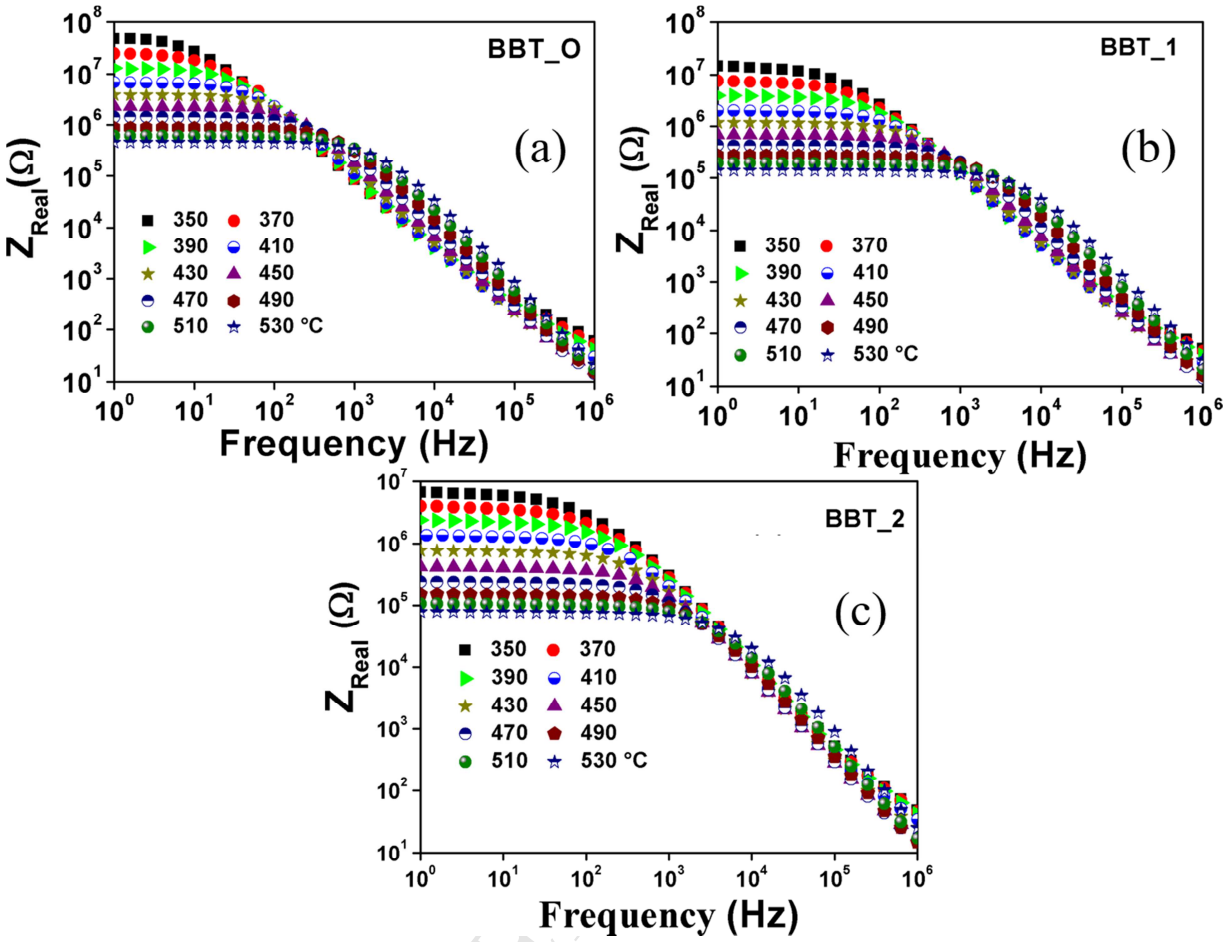

Figure 3 -Temperature dependence of the real part of impedance (Z_{real}) with frequency in different temperature for (a) BBT_O; (b) BBT_1; and (c) BBT_2.

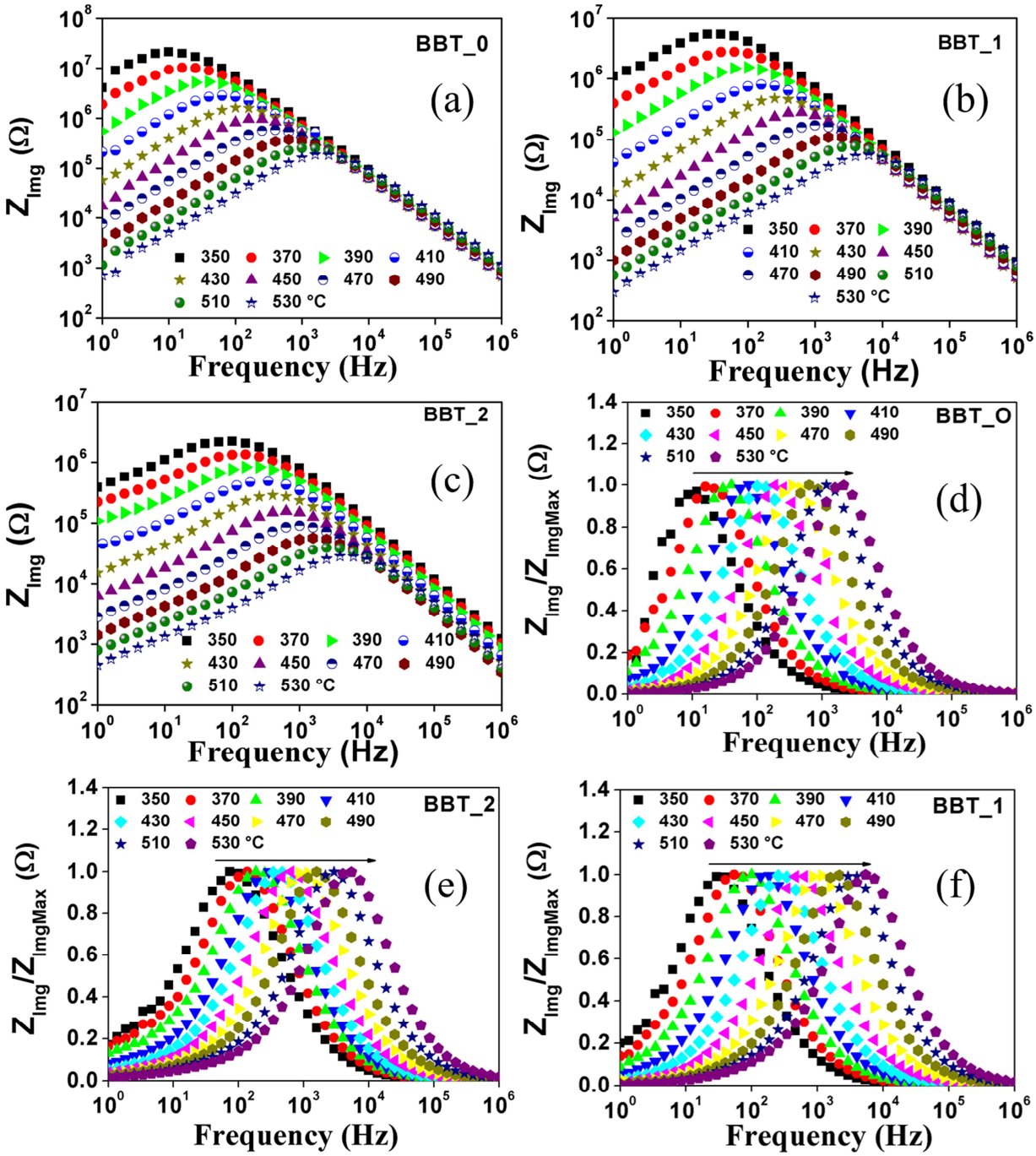

Figure 4 - (a-c) shows the temperature dependence of the imaginary part of impedance (Z_{Imgl}) with frequency in different temperature and (d-f) normalization of the imaginary impedance component for BBT_O, BBT_1 and BBT_2.

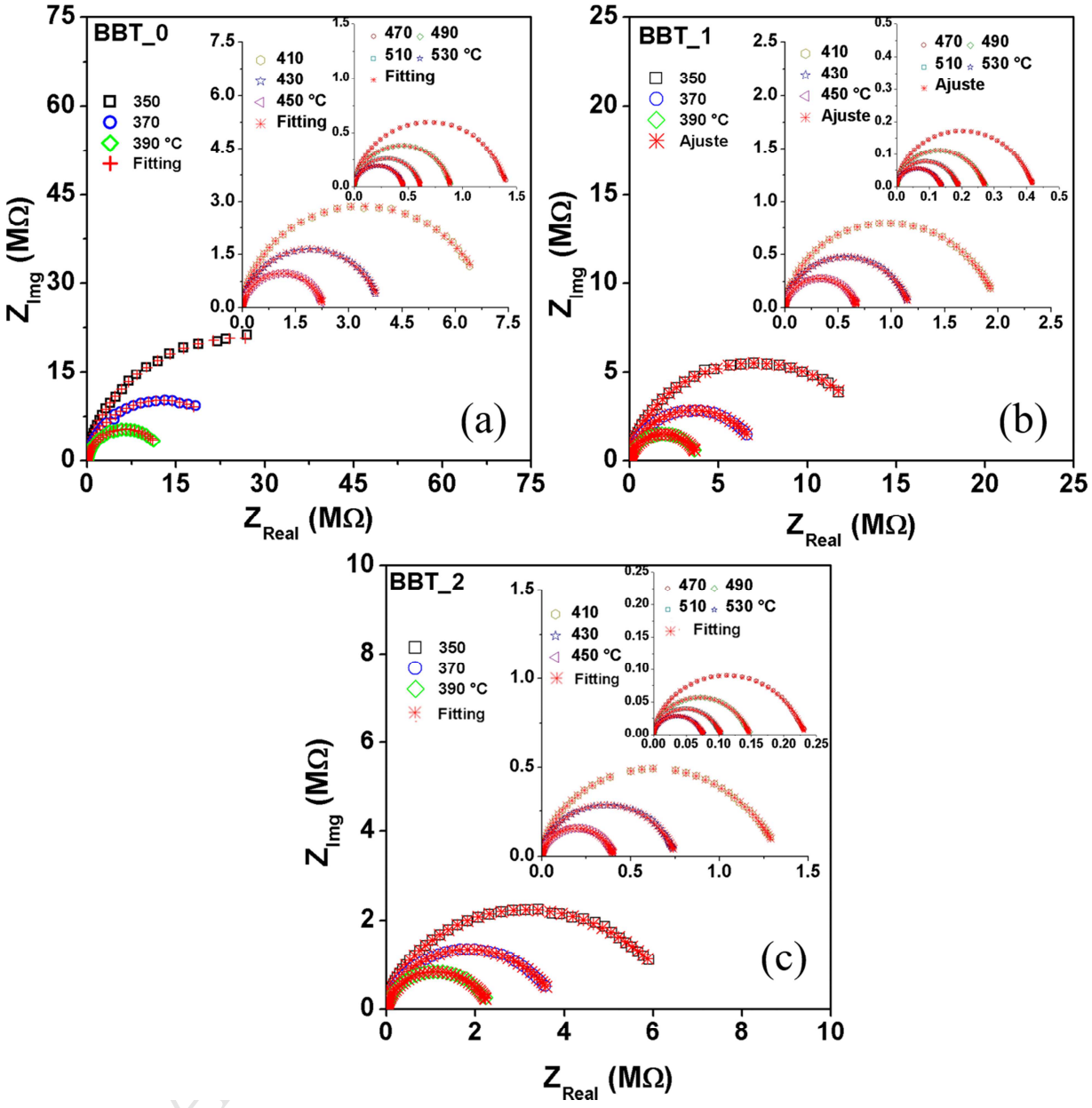

Figure 5 - (a-c) Experimental and calculated (symbols +) using the equivalent circuit to plots of Z_{Real} versus Z_{Img} at different temperature for BBT_O, BBT_1 and BBT_2.

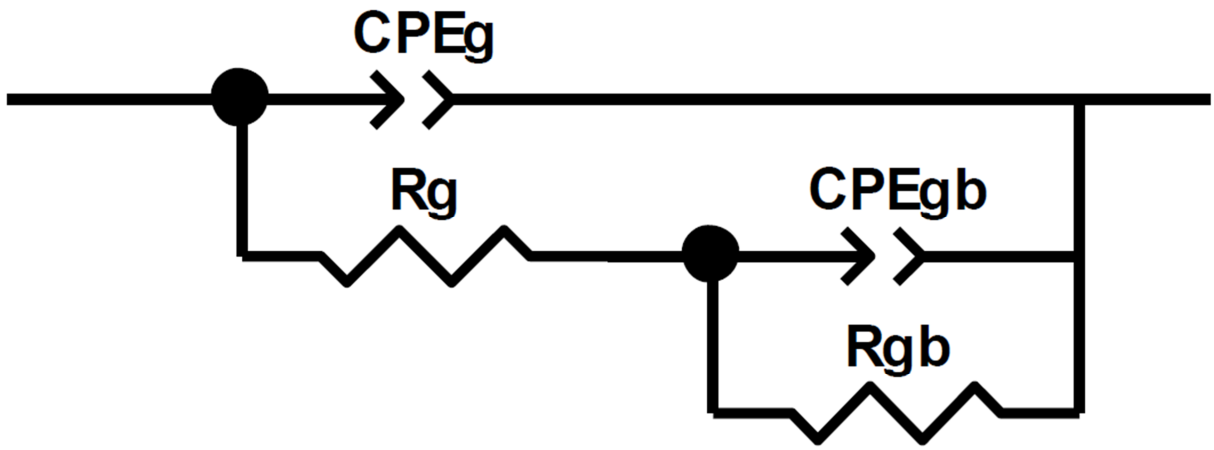

Figure 6 - Diagram of the equivalent circuit to analyze the experimental results.

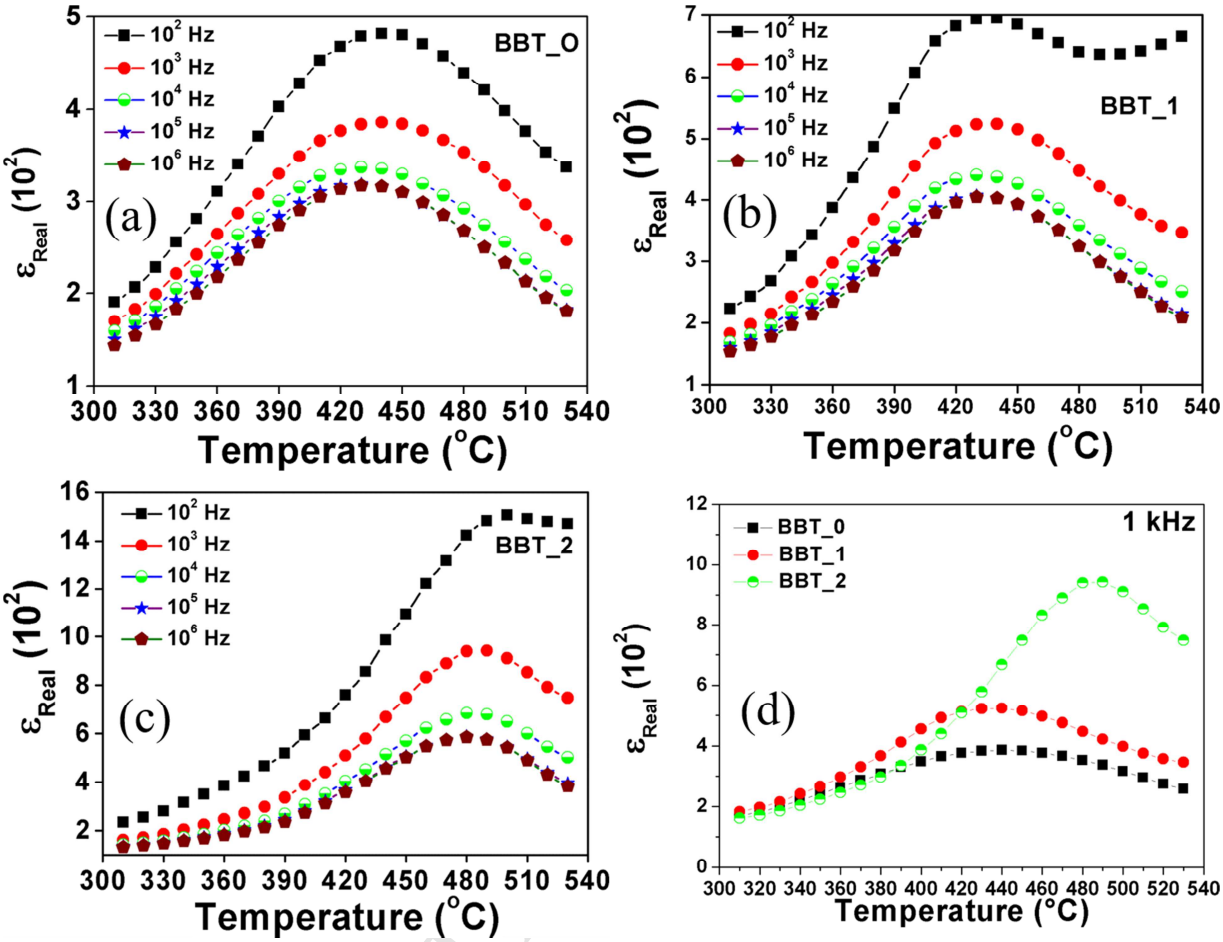

Figure 7 - (a-d) – Temperature and frequency dependence of dielectric constant (ε_{Real}) for BBT_O, BBT_1 and BBT_2.

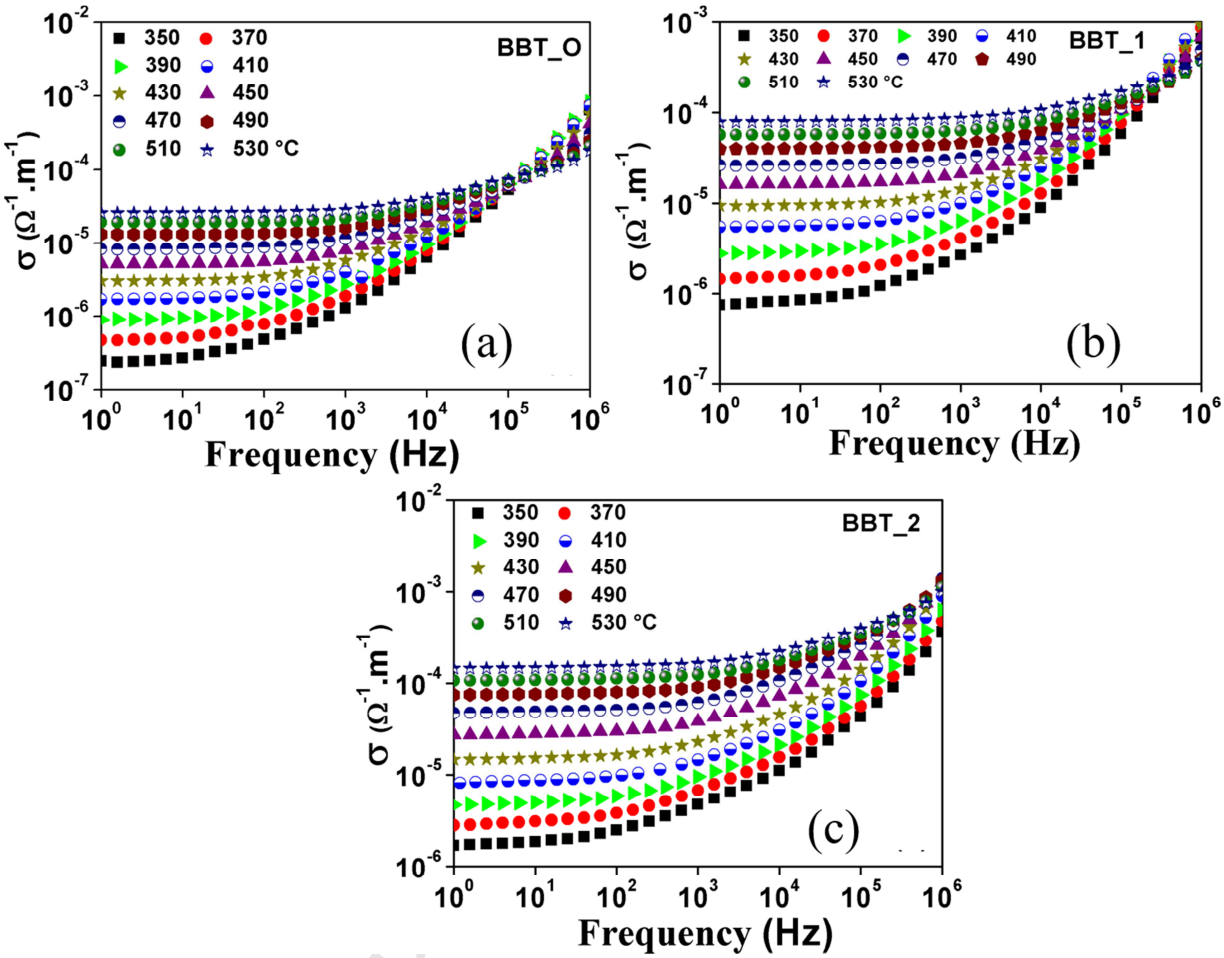

Figure 8 - (a-c) Variation of σ as a function of frequency at different temperature for BBT_O, BBT_1 and BBT_2.

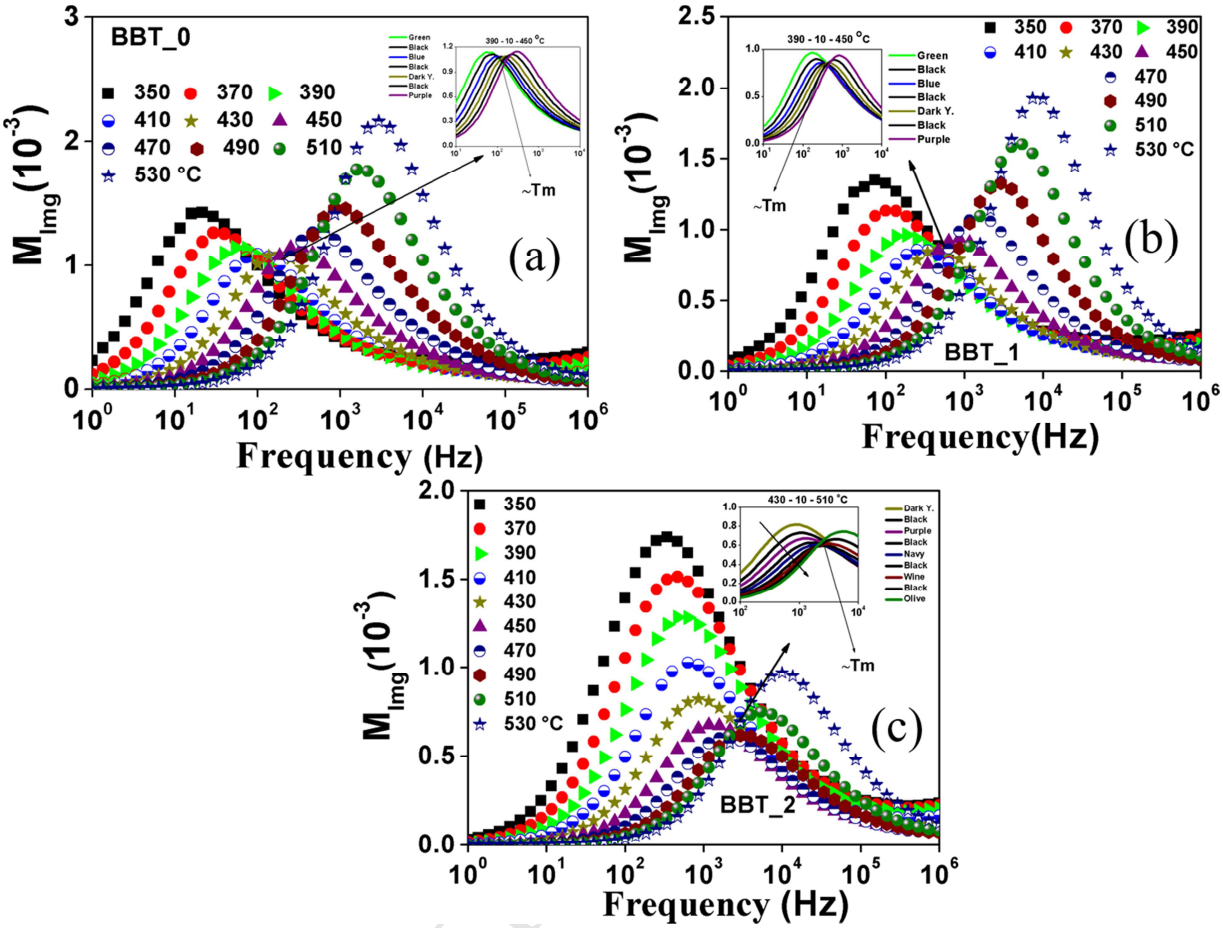

Figure 9 - (a-c) Variation of M_{Img} with frequency at different temperature for BBT_O, BBT_1 and BBT_2.

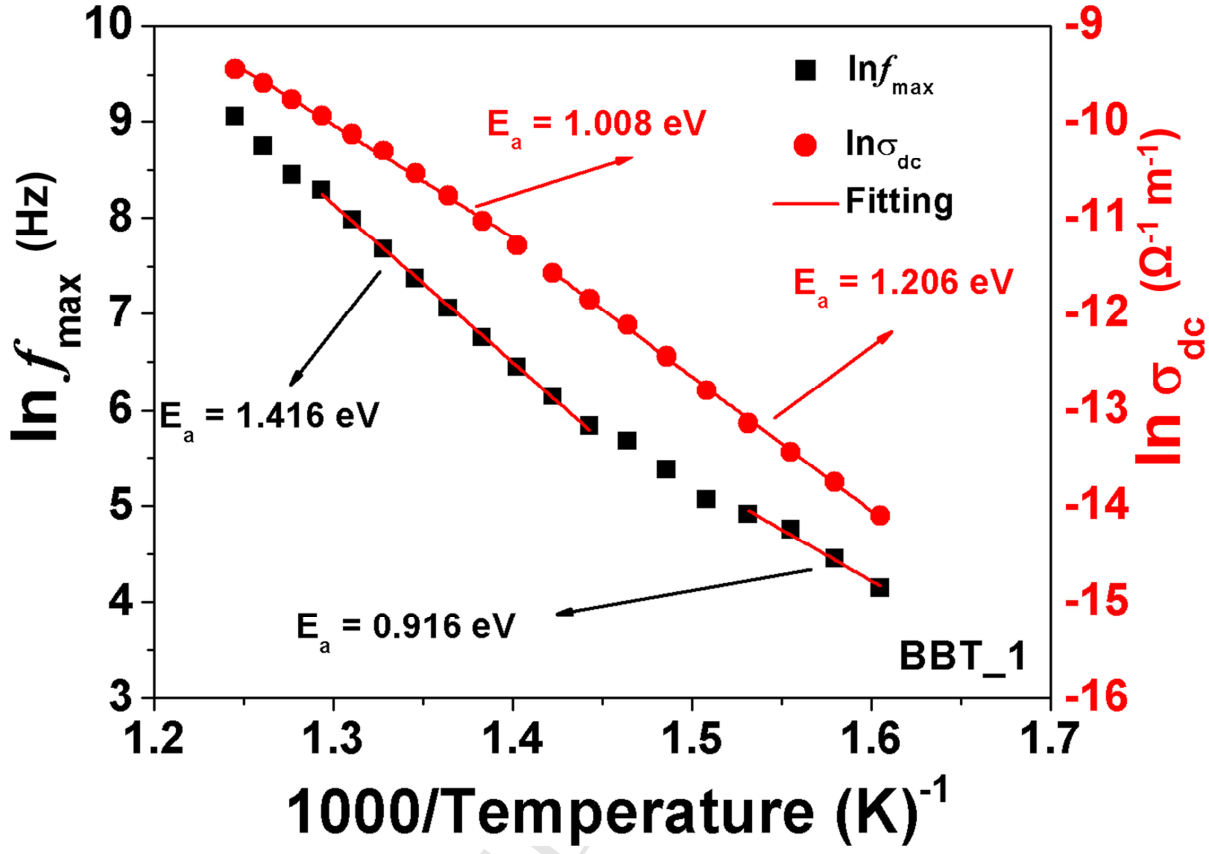

Figure 10 -The Arrhenius plots for BBT_1 shows dependence σ_{dc} conductivity and f_{max}(peak) versus inverse of absolute temperature.

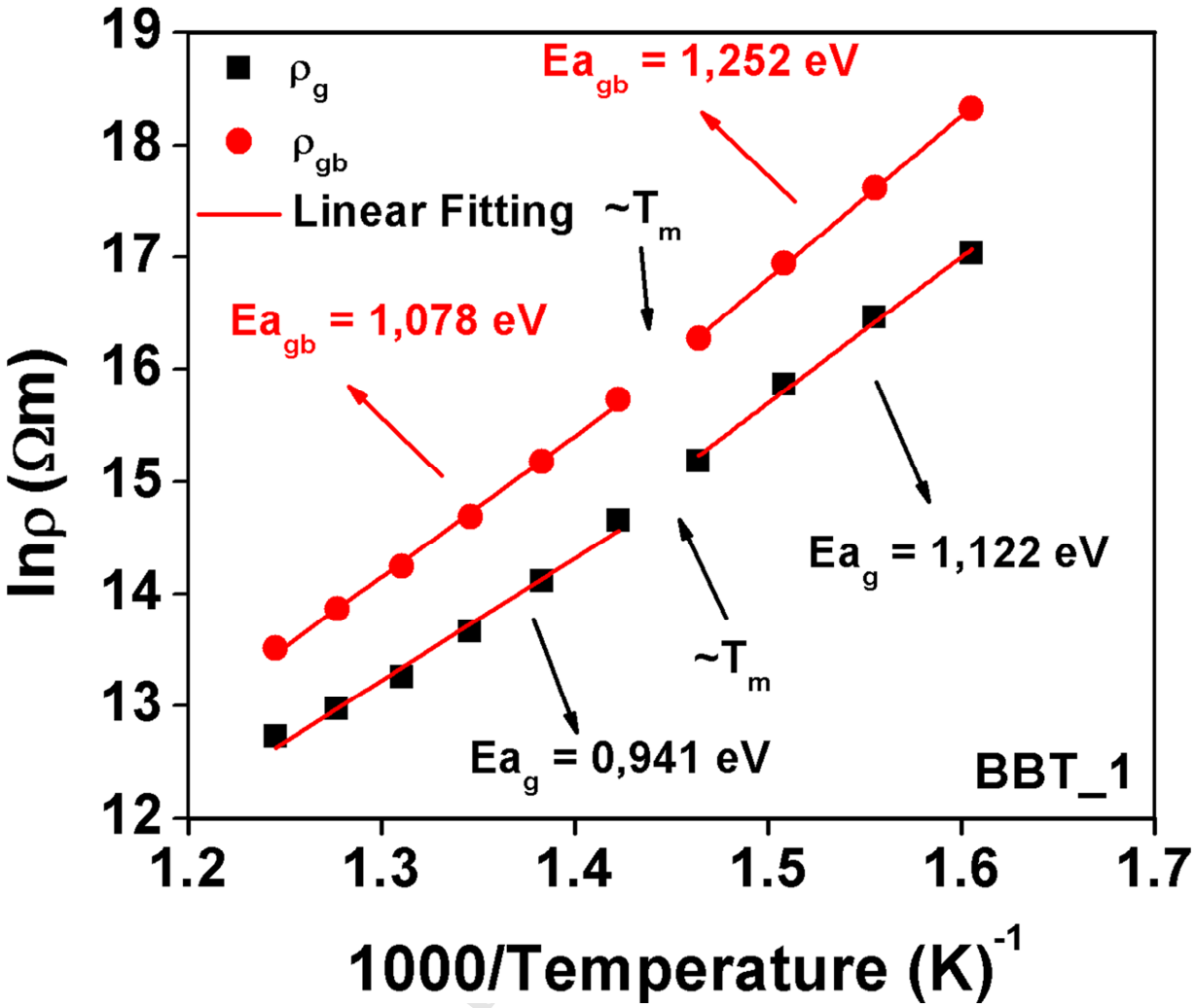

Figure 11 -The Arrhenius plots for BBT_1 shows dependence resistivity (ρ) versus inverse of absolute temperature.

Research highlights

- $BaBi_4Ti_4O_{15}$ ceramics doped with magnesium oxide (1-5%)
- Formation of the orthorhombic phase
- Decrease in the unit cell volume was due to insertion of Mg^{2+} into Ti^{4+} sites
- Increase of magnesium oxide amount there was a decrease in the value of the complex impedance
- Equivalent circuit including the contribution of grain and grain-boundaries